Correlation between coherent Jahn-Teller distortion and magnetic spin orientation in $La_{1-x}Sr_xMnO_3$

X. Xiong, B. Dabrowski, O. Chmaissem, Z. Bukowski, S. Kolesnik, R. Dybzinski, and C. W. Kimball
Department of Physics, Northern Illinois University, DeKalb, Illinois 60115

J. D. Jorgensen
Materials Science Division, Argonne National Laboratory, Argonne, Illinois 60439
(Received 20 May 1999)

The magnetic structure and its correlation with the Jahn-Teller (JT) distortion in lightly doped $La_{1-x}Sr_xMnO_3$ ($0.11 \leqslant x \leqslant 0.185$) have been studied as a function of temperature from 10–300 K using neutron powder diffraction. A correlation between the ferromagnetic spin orientation and the coherent JT distortion was observed, indicating a coupling between the structural and the magnetic properties. The arrangement of the spins varies from ferromagnetic ordered mainly along the *b* axis ($x=0.11$) to ferromagnetic almost along the *c* axis ($x=0.185$) in the *Pbnm* symmetry. [S0163-1829(99)07237-9]

INTRODUCTION

Structural effects, such as strong Jahn-Teller (JT) type electron-phonon coupling, the average ionic radius of La site, and cation disorder effects, have been demonstrated to affect the magnetoresistive properties of the manganese oxide perovskites $R_{1-x}M_xMnO_3$ ($R=$La, Pr, Nd; $M=$Ca, Sr).[1–8] For stoichiometric $LaMnO_3$, the orthorhombic *Pbnm* structure below $T=750$ K is characterized by a large JT distortion which breaks the degeneracy of the electronic configuration of the Mn^{3+} ions ($t_{2g}^3e_g^1$). $La_{1-x}M_xMnO_3$ transforms from an antiferromagnetic insulator to a ferromagnetic metal as Sr or Ca substitution is increased. The ferromagnetic ordering is mediated by a double exchange mechanism.[9–11] On substitution of La with Sr or Ca, Mn^{3+} ions change to the Mn^{4+} state without e_g electrons. The e_g electrons of the Mn^{3+} ions gain kinetic energy to overcome the loss of the exchange energy of the t_{2g} spins and hop into the vacant e_g state of the Mn^{4+} ions, which eventually results in metallic ferromagnetism. Subsequent to the pioneering magnetic structure study by Wollan and Koehler,[12] who described several basic antiferromagnetic, canted-antiferromagnetic, and ferromagnetic structures in the $La_{1-x}Ca_xMnO_3$ system, several neutron diffraction studies have been performed to investigate the magnetic structure for the $La_{1-x}M_xMnO_3$ system.[13–16] Stoichiometric $LaMnO_3$ has a commensurate layer-type (*A*-type) antiferromagnetic structure with the moments parallel to the *b* axis and the antiferromagnetic propagation vector along the *c* axis in *Pbnm* symmetry.[12,16] The ferromagnetic component grows gradually on the *A*-type antiferromagnetic matrix as the Sr or Ca substitution increases, resulting in a canted-antiferromagnetic phase. The ferromagnetic component suddenly dominates over the antiferromagnetic component for $x \geqslant \sim 0.15$ in $La_{1-x}Ca_xMnO_3$,[12] and for $x \geqslant \sim 0.09$ in $La_{1-x}Sr_xMnO_3$.[16] A recently proposed spiral spin structure,[17] which was thought to be energetically more favorable than the canted antiferromagnetic state for low hole hopping *x*, was not confirmed experimentally because only the magnetic peaks, at either the antiferromagnetic (AF) position $(0, \pi, 0)$ or the ferromagnetic (F) position (0, 0, 0), were observed.[16] The spiral spins should produce a set of magnetic superstructure reflections which vary from AF $(0, \pi, 0)$ to F (0, 0, 0) depending on the period of the magnetic super unit cell.

Neutron-diffraction studies on the $La_{1-x}Sr_xMnO_3$ system have shown that the ferromagnetic ordering strongly suppresses the coherent JT distortion for $0.1 \leqslant x \leqslant 0.17$.[18–20] This indicates a strong coupling among structural distortion, ferromagnetic ordering, and transport properties. A structural phase transition and associated insulator-metal transition induced by an external magnetic field was found in $La_{1-x}Sr_xMnO_3$ ($x=0.17$), providing evidence for strong coupling of the local spin moments and the charge carriers to the crystal lattice.[21] In addition, a relationship was established among the electronic, spin, and local MnO_6 distortions in $La_{1-x}Ca_xMnO_3$ by a recent x-ray-absorption fine-structure study.[22]

We report here detailed refinements of the ferromagnetic structures for $La_{1-x}Sr_xMnO_3$ ($0.11 \leqslant x \leqslant 0.185$) as a function of both hole concentration and temperature. We show that the orientation of the ferromagnetic spin moments is correlated with the magnitude of the coherent JT distortion. For the ferromagnetic compositions, the spins are mainly pointed along the *b* axis when the residual coherent JT distortion is relatively large, and align almost along the *c* axis as the coherent JT distortion disappears due to the hole doping.

SAMPLE PREPARATION AND CHARACTERIZATIONS

Polycrystalline samples of $La_{1-x}Sr_xMnO_3$ ($x=0.10-0.20$) were synthesized using a wet chemistry method.[23] Stoichiometric material was obtained by firing in air at ~1400 °C for a day, followed by a fast cooling to room temperature on a Cu plate. The wet-chemistry method leads to dense samples with homogenous mixing of Sr and La ions on the *A* site.

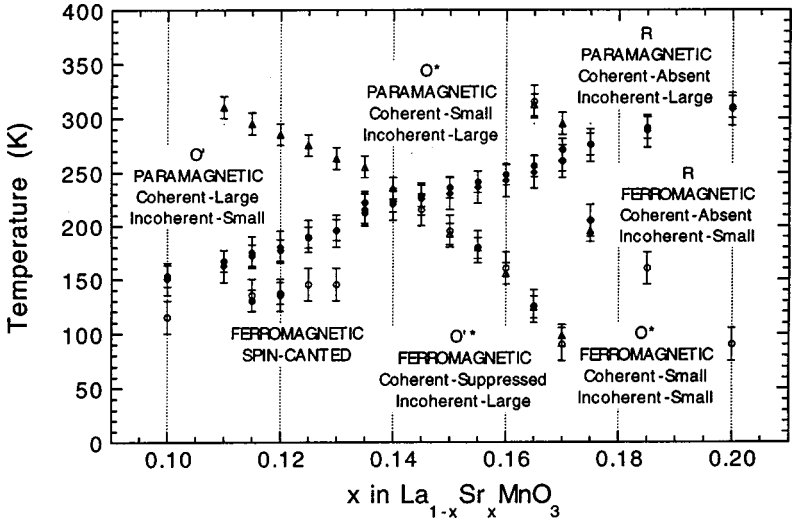

FIG. 1. Phase diagram summarizing the magnetic and structural properties of $La_{1-x}Sr_xMnO_3$ as a function of composition, $0.11 \leqslant x \leqslant 0.2$, and temperature, $12 \leqslant T \leqslant 350$ K. (From Ref. 23.) The solid diamond points, from ($x=0.10$, $T=150$ K) to ($x=0.20$, $T=310$ K), form the ferromagnetic ordering transition (T_c) line. The empty triangle points, from ($x=0.11$, $T=310$ K) to ($x=0.17$, $T=100$ K), form the coherent Jahn-Teller distortion transition (T_{JT}) line. O^*, O', O'^*, and R stand for the small coherent JT-distorted orthorhombic ($\sigma_{JT} \sim 0.004$ Å), large coherent JT-distorted orthorhombic ($\sigma_{JT} \sim 0.05$ Å), suppressed coherent JT-distorted orthorhombic ($\sigma_{JT} \sim 0.02$ Å), and the rhombohedral phases, respectively. σ_{JT} is the Jahn-Teller distortion parameter defined in text.

Magnetic and resistive properties of these samples at small magnetic fields were reported previously and the results were combined with the neutron powder-diffraction data to construct a detailed phase diagram of magnetic and structural properties as shown in Fig. 1 (i.e., Fig. 1 of Ref. 23). Magnetization measurements in applied magnetic fields were performed using a Quantum Design Physical Properties Measurement System, Model 6000, equipped with a dc magnetometer. Figure 2 shows magnetization as a function of temperature measured in 1, 3, 5, and 7 T fields for the $La_{0.815}Sr_{0.185}MnO_3$ sample. With increasing magnetic field, the $M(T)$ curves show typical features of a ferromagnet; i.e., increased transition temperatures and shapes predicted approximately by the spin-wave theory.[24] Similar measurements for most compositions have shown that the temperature dependence of the magnetization below $\sim(1/2)T_c$ at high magnetic fields can be very well described by the predicted formula:

$$M(T) = M(0) - a(T/T_c)^{3/2}. \tag{1}$$

However, for several samples near $x \approx 0.125$, a clear kink at 125–145 K was visible, indicating a magnetic transition. The kinks in high-field magnetization appear near the temperatures where a decrease-magnetization anomaly was observed at small magnetic fields.[23] The persistence of this anomaly at high fields may indicate that it is related to a spin canting transition.[19] Most probably, it is not caused by a charge-density wave[25] or by domain structure changes. Because of the proximity of the ferromagnetic and structural transitions at these compositions, this transition is difficult to study and it is still under investigation with ac susceptibility, magnetostriction, and local probe measurements.

The inset to Fig. 2 shows magnetization as a function of magnetic field at 6 K for the $La_{0.815}Sr_{0.185}MnO_3$ sample. For this and similar compositions at low temperatures, the magnetization saturates at fields of about 3 T. Slightly larger fields, up to 5 T, were necessary to achieve a full saturation for smaller $x=0.10-0.15$. Figure 3 shows the derived magnetic moment per Mn ion as a function of x. The measured magnetic moment decreases with increasing substitution by Sr in agreement with removal of electrons from the e_g^1 orbital that originates from the charge doping. The agreement among the measured (solid line) and calculated [broken line, μ (calculated)$=(1-x)(4\mu_B)+x(3\mu_B)$] is very good confirming that the spin-orbit coupling is very weak for ferromagnetic manganites.[26]

Neutron powder-diffraction patterns were measured for

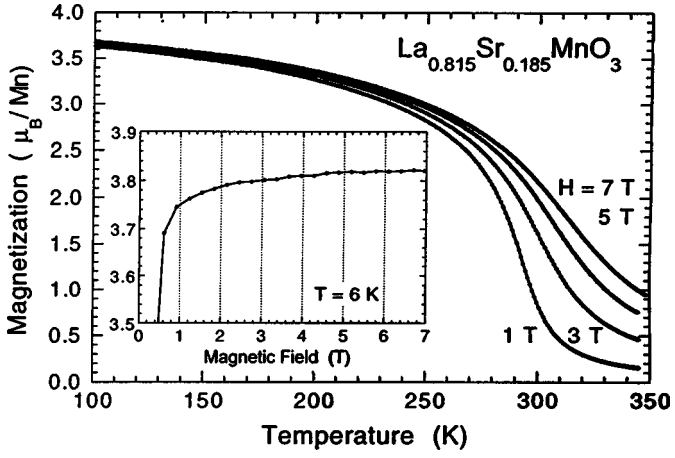

FIG. 2. Magnetization as a function of temperature measured in 1, 3, 5, and 7 T for the $La_{0.815}Sr_{0.185}MnO_3$ sample. The inset shows the magnetization as a function of magnetic field at 6 K for the $La_{0.815}Sr_{0.185}MnO_3$ sample.

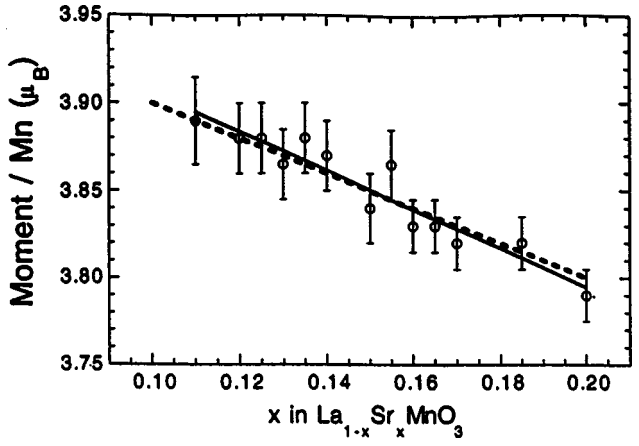

FIG. 3. The derived magnetic moment per Mn ion as a function of x in $La_{1-x}Sr_xMnO_3$.

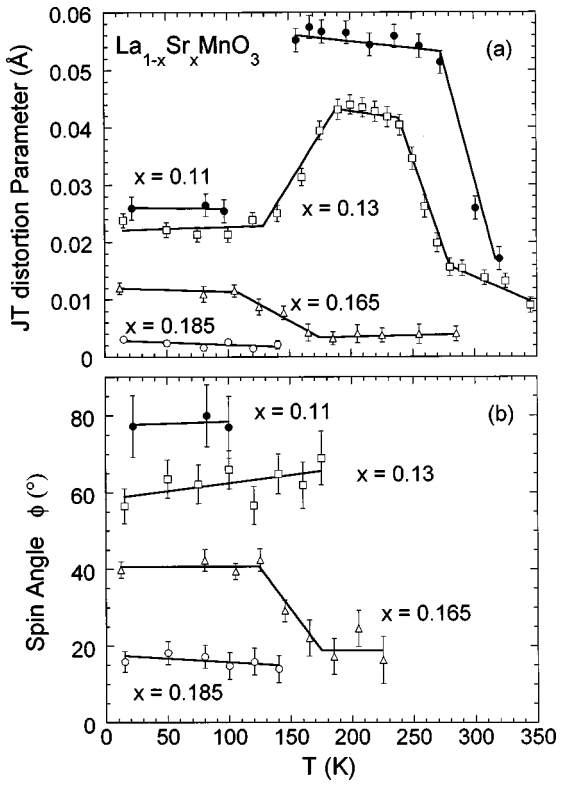

FIG. 4. The Jahn-Teller distortion parameter σ_{JT} (a) and the refined spin orientation ϕ (b) as a function of temperature for $La_{0.89}Sr_{0.11}MnO_3$, $La_{0.87}Sr_{0.13}MnO_3$, $La_{0.835}Sr_{0.165}MnO_3$, and $La_{0.815}Sr_{0.185}MnO_3$.

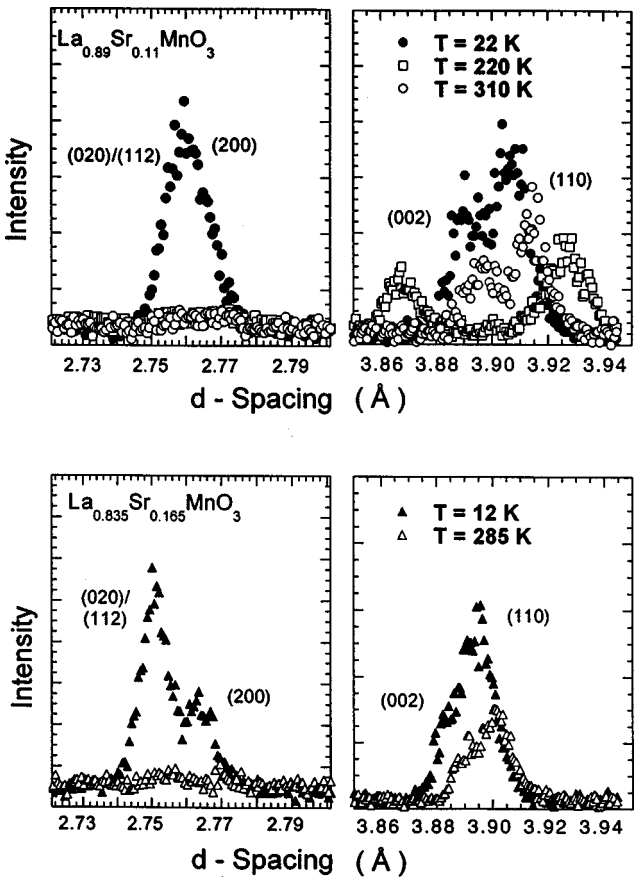

FIG. 5. The diffracted intensities above and below T_c for $La_{0.89}Sr_{0.11}MnO_3$ and $La_{0.835}Sr_{0.165}MnO_3$.

$x=0.11$, 0.13, 0.165, and 0.185 using the Special Environment Powder Diffractometer at Argonne's Intense Pulsed Neutron Source.[27] Data were collected on all detector banks, but only the higher resolution backscattering data ($\Delta d/d = 0.035$) were analyzed. Diffraction patterns were analyzed by the Rietveld method using the GSAS program.[28] In these refinements, data were analyzed over the *d*-spacing range of 0.4–4 Å. The background was modeled using an eight-term cosine Fourier series and diffraction peaks were described using a two-sided exponential that was convoluted with a Gaussian and a Lorentian to describe the instrumental and sample contribution to the peak profile, respectively. Lattice parameters, atom positions, magnetic moments, and Debye-Waller factors were refined.

RESULTS AND DISCUSSIONS

$La_{1-x}Sr_xMnO_3$ ($0.0 \leqslant x < 0.17$) has an orthorhombic structure with space group *Pbnm* at room temperature. The unit cell is $\sqrt{2}a_p \times \sqrt{2}a_p \times 2a_p$ (where a_P is the cubic lattice parameter) of the primitive perovskite cell. This orthorhombic *Pbnm* space group has one apical and two equatorial oxygen sites, which define a distortion of the MnO_6 octahedra and a distribution of Mn-O bond lengths, i.e., one apical bond (Mn-O_a) and two equatorial bonds (Mn-O_{e1} and Mn-O_{e2}). The orthorhombic structure shows a relatively large coherent JT distortion (the O' phase) or very small coherent JT distortion (the O^* phase) depending on temperature and hole concentration.[19,20] It was further determined that the ferromagnetic ordering suppresses the coherent JT distortion.[18–20] The rhombohedral structure with space group $R\bar{3}c$ in its hexagonal description appears for $x>0.17$ for $La_{1-x}Sr_xMnO_3$ at room temperature.

In Fig. 1, upon decreasing temperature, the coherent JT distortion transition (T_{JT}) precedes the ferromagnetic ordering (T_c) for $x<0.145$, whereas T_c precedes T_{JT} for $x>0.145$. The two transition lines cross at $x\sim0.145$, where both the coherent JT distortion transition and the ferromagnetic ordering appear at the same temperature. The two transition lines separate four different regions where the coherent and incoherent JT distortions form differently. For $x<0.145$, the JT distortion is incoherent and the MnO_6 octahedra are locally or dynamically distorted above T_{JT},[29] while below T_{JT}, the coherent JT distortion is large above T_c but much suppressed below T_c. For $0.145<x<0.175$, the incoherent JT distortion is suppressed at T_c, and the coherent JT distortion transition well below T_c is much weaker than that for $x<0.145$. Therefore for $0.145<x<0.17$, on cooling below room temperature, one should observe three distinct JT-distorted phases, i.e., a paramagnetic O^* phase with a small coherent JT distortion and a large incoherent JT distortion, a ferromagnetic O^* phase with a small coherent JT distortion and a small incoherent JT distortion, and a ferromagnetic O'^* phase with a suppressed coherent JT distortion. The weak coherent JT distortion transition in the ferromagnetic region was not observed for $x>0.175$ below T_c.

Before discussing the magnetic structure, it is useful to define the coherent JT distortion parameter σ_{JT}:

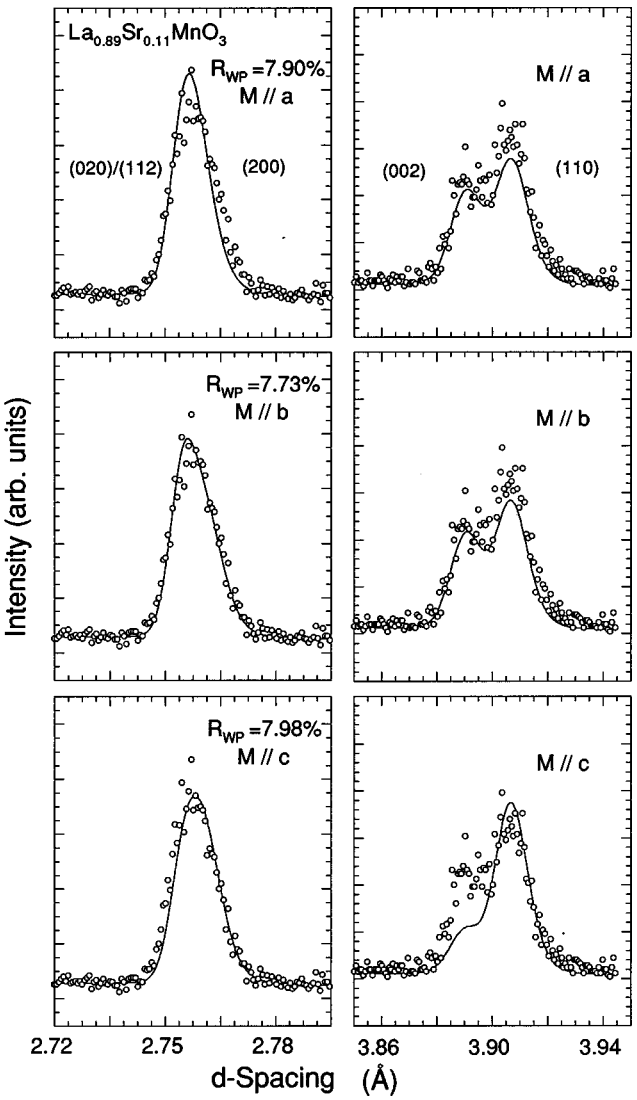

FIG. 6. Refined intensities and experimental data at 12 K for models with the ferromagnetic spin direction along the *a*, *b*, and *c* axes, respectively, for $La_{0.89}Sr_{0.11}MnO_3$. Goodness of fit parameters R_{WP} are shown for each fit.

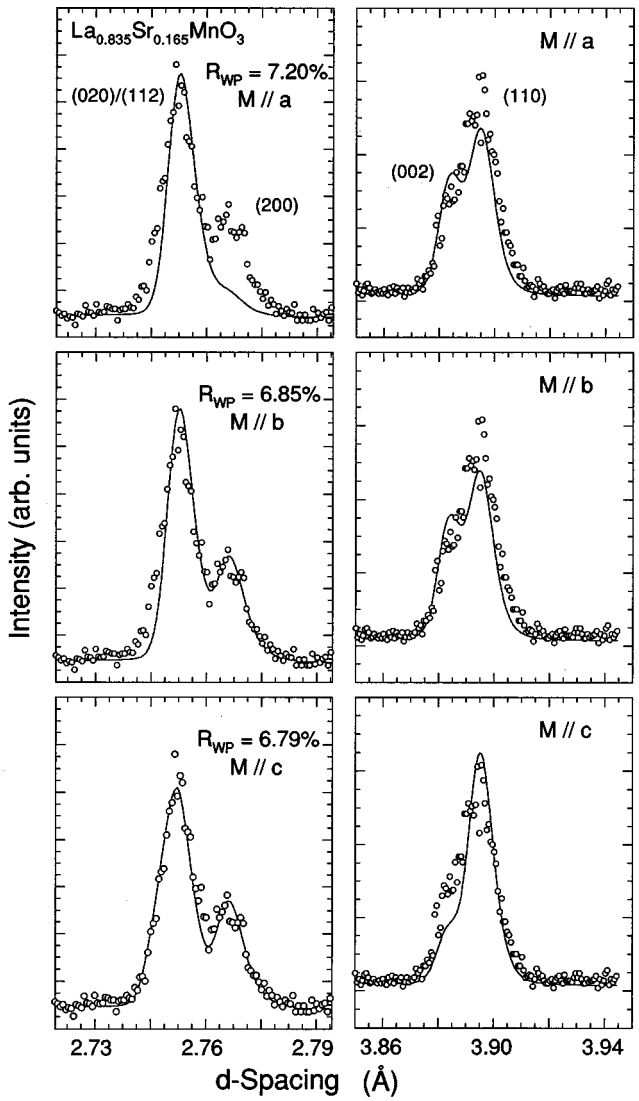

FIG. 7. Refined intensities and experimental data at 12 K for models with the ferromagnetic spin direction along the *a*, *b*, and *c* axes, respectively, for $La_{0.835}Sr_{0.165}MnO_3$. Goodness of fit parameters R_{WP} are shown for each fit.

$$\sigma_{\mathrm{JT}}=\sqrt{\tfrac{1}{3}\sum_i\left[(\mathrm{Mn-O})_i-\langle\mathrm{Mn-O}\rangle\right]^2}, \tag{2}$$

where $(\mathrm{Mn\text{-}O})_i$ stands for the three independent Mn-O bond lengths. Figure 4(a) shows the temperature dependence of the JT distortion parameters σ_{JT} for $La_{0.89}Sr_{0.11}MnO_3$, $La_{0.87}Sr_{0.13}MnO_3$, $La_{0.835}Sr_{0.165}MnO_3$, and $La_{0.815}Sr_{0.185}MnO_3$. Upon decreasing temperature, the coherent JT distortion sets in at ~310 K for $La_{0.89}Sr_{0.11}MnO_3$, and at ~280 K for $La_{0.87}Sr_{0.13}MnO_3$. σ_{JT} decreases at the ferromagnetic ordering temperature T_c, 170 K for $La_{0.89}Sr_{0.11}MnO_3$ and 200 K for $La_{0.87}Sr_{0.13}MnO_3$, which results in a suppressed coherent JT-distorted phase O'^* as shown in Fig. 1. Two phases, the O' and O'^* phases, coexist from 150–120 K in $La_{0.89}Sr_{0.11}MnO_3$ and the data points within this range are not shown in Fig. 4(a). σ_{JT} for $La_{0.835}Sr_{0.165}MnO_3$ is, however, much smaller, ~0.004 Å at 285 K, and stays constant at $T_c=255$ K but increases below 160 K, indicating a weak coherent JT distortion transition (from O^* to O'^*) in the ferromagnetic region.[23] $La_{0.815}Sr_{0.185}MnO_3$ is rhombohedral at room temperature with a ferromagnetic ordering temperature $T_c=290$ K. The transition temperature from the rhombohedral to orthorhombic structure is 150 K as determined in Ref. 23. From 150–12 K, the orthorhombic structure has a very small coherent JT distortion ($\sigma_{\mathrm{JT}}=0.003$ Å), and an additional weak coherent JT distortion transition in the ferromagnetic region is not observed.

The magnetic structure factor can be written as

$$\mathbf{F}_m(\mathbf{q})\propto\sum_j\{\hat{q}\times\langle\mathbf{S}_j\rangle\times\hat{q}\}f(\mathbf{q})e^{i\mathbf{q}\cdot\mathbf{r}_j}e^{-w_j}, \tag{3}$$

where S_j is the spin at site j. The magnetic form factor $f(\mathbf{q})$ accounts for the spacial distribution of unpaired electron spins and leads to a falloff of intensities at large $|\mathbf{q}|$ or low d spacing. The vector product of the spin direction $\mathbf{S}$ and wave vector $\mathbf{q}$ in Eq. (3) determines the magnetic intensity. For

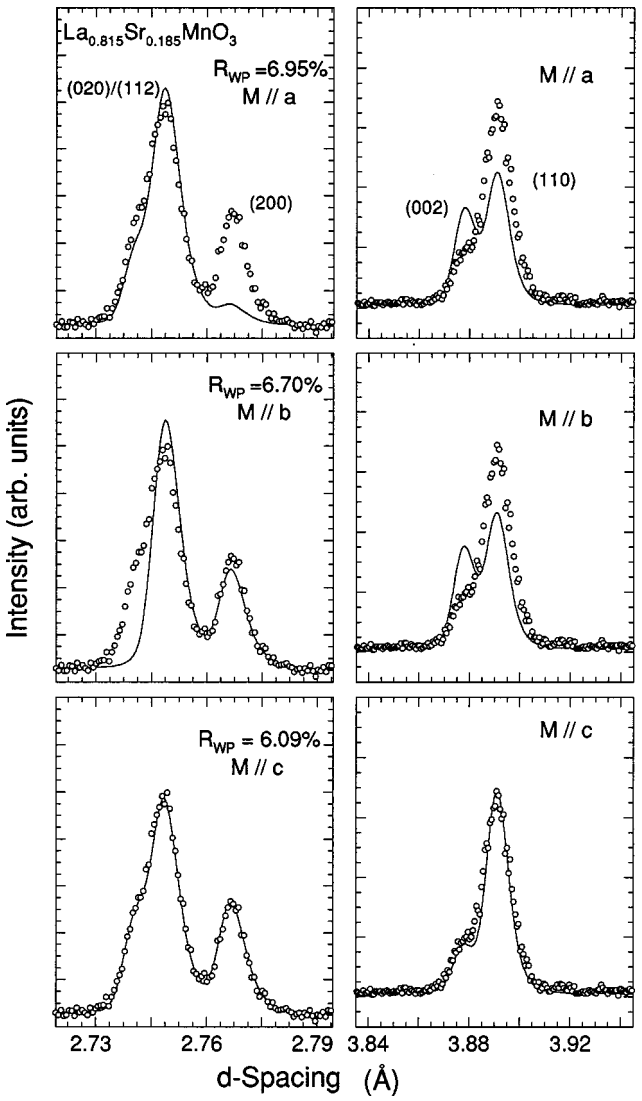

FIG. 8. Refined intensities and experimental data at 12 K for models with the ferromagnetic spin direction along the *a*, *b*, and *c* axes, respectively, for $La_{0.815}Sr_{0.185}MnO_3$. Goodness of fit parameters R_{WP} are shown for each fit.

example, if the spin is along the *c* axis, the magnetic intensity vanishes at the $(00l)$ peaks.

As we mentioned earlier, $LaMnO_3$ has an *A*-type antiferromagnetic structure with the propagation vector [001] and the spin moment along the *b* axis in the *Pbnm* symmetry.[12,16] The ferromagnetic component (along the *c* axis) grows on the *A*-type antiferromagnetic matrix as the hole concentration (x) increases, and the resulting magnetic space group is $Pb'n'm$.[12,16] The sharp crossover from the canted-antiferromagnetic (CAF) structure to a ferromagnetic (F) structure was reported to occur at $x\sim0.15$ for $La_{1-x}Ca_xMnO_3$, and at $x\sim0.09$ for $La_{1-x}Sr_xMnO_3$,[12,16] respectively. As the hole concentration goes beyond the CAF-F boundary, at $x\sim0.09$ for $La_{1-x}Sr_xMnO_3$, the exact ferromagnetic spin orientation and its relation to the coherent JT distortion were not determined in previous work. We focus on this issue next.

Figure 5 shows the (020), (112), (200), (002), and (110) reflections above and below T_c for $La_{0.89}Sr_{0.11}MnO_3$ and $La_{0.835}Sr_{0.165}MnO_3$. It is noted that the measured intensity below T_c includes both the nuclear and the magnetic intensities, while only the nuclear intensities contribute above T_c. The magnetic intensities are thus the difference between the total intensities and the nuclear intensities. The magnetic peaks (020), (112), and (200) have negligible nuclear structure factors as indicated by the undetectable intensity above T_c. The ferromagnetic intensity was, however, observed to be comparable to the nuclear intensity at (002) and (110) below T_c. It is necessary to measure magnetic peaks along all of the (100), (010), and (001) directions to determine the ferromagnetic structure according to Eq. (3).

Figures 6–8 show the refined intensities and associated R_{WP}'s and experimental data at $\sim$12 K for models of the magnetic structure with the spin direction along the *a*, *b*, and *c* axes, respectively, for $La_{0.89}Sr_{0.11}MnO_3$ (Fig. 6), $La_{0.835}Sr_{0.165}MnO_3$ (Fig. 7), and $La_{0.815}Sr_{0.185}MnO_3$ (Fig. 8). The standard magnetic space groups are $Pbn'm'$, $Pb'nm'$, and $Pb'n'm$ for the spins along the *a*, *b*, and *c* axes, respectively.[30] Of these models for the spin orientation, the best agreement as indicated by the smallest R_{WP}, is for spin orientation along the *b* axis for $La_{0.89}Sr_{0.11}MnO_3$, along the *c* axis for $La_{0.835}Sr_{0.165}MnO_3$, and along the *c* axis for $La_{0.815}Sr_{0.185}MnO_3$. However, the (002) intensity is not modeled well for $La_{0.835}Sr_{0.165}MnO_3$. According to Eq. (3), only the *a* or *b* component of a spin vector should contribute intensity to the (002) peak for $La_{0.835}Sr_{0.165}MnO_3$. Indeed, an improved refinement (shown in Fig. 9) is achieved by tilting the ferromagnetic moment by an angle of ϕ away from the *c* axis in the *bc* plane for $La_{0.835}Sr_{0.165}MnO_3$. The magnetic unit cell is depicted in the inset of Fig. 9. The magnetic space group is constructed by using space group $P1$ because all the basic orthorhombic symmetry elements are violated by our ferromagnetic model with tilted spins. The spin orientation angle ϕ is defined as the angle between the ferromagnetic moment (in the *bc* plane) and the *c* axis as shown in the inset of Fig. 9. The ferromagnetic components along the *b* axis and along the *c* axis are refined to be M_b and M_c, respectively. ϕ is then determined by $\tan(\phi)=M_b/M_c$. These refinements suggest that the spin orientation changes with the hole concentration from $x=0.11-0.185$ in $La_{1-x}Sr_xMnO_3$ at 12 K.

As we discussed earlier, the increased hole doping leads to a reduction of the coherent JT distortion parameter σ_{JT}. One then is led to expect a correlation between the spin orientation and the coherent JT distortion, which is indeed revealed in Fig. 4. Figure 4 shows the refined spin angle ϕ [Fig. 4(b)] and the calculated coherent JT distortion parameter σ_{JT} [Fig. 4(a)] as a function of the temperature and hole doping x in $La_{1-x}Sr_xMnO_3$. The refined spin angle and coherent JT distortion basically remains constant below T_c for $La_{0.89}Sr_{0.11}MnO_3$, $La_{0.87}Sr_{0.13}MnO_3$, and $La_{0.815}Sr_{0.185}MnO_3$, except for $La_{0.835}Sr_{0.165}MnO_3$ in which a weak coherent JT distortion transition occurs at 160 K. We will discuss $La_{0.835}Sr_{0.165}MnO_3$ in detail in the next section. The spin is aligned almost along the *b* axis in $La_{0.89}Sr_{0.11}MnO_3$ ($\phi\sim77°$) with a residual coherent JT distortion $\sigma_{JT}=0.026$ Å at 20 K. The spin angle decreases to 57° and 40° for $La_{0.87}Sr_{0.13}MnO_3$ and $La_{0.835}Sr_{0.165}MnO_3$ at $\sim$12 K, respectively. The corresponding residual σ_{JT} also decreases to 0.024 and 0.012 Å for $La_{0.87}Sr_{0.13}MnO_3$ and $La_{0.835}Sr_{0.165}MnO_3$ at 12 K, respectively. The spin rotates to

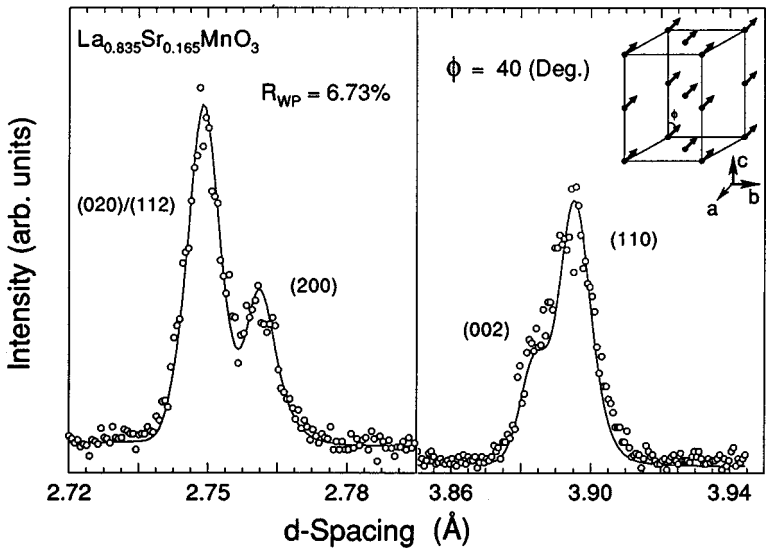

FIG. 9. Measured and calculated intensities when the spin angle ϕ was refined to be 40° for $La_{0.835}Sr_{0.165}MnO_3$ at 12 K. The inset shows the magnetic unit cell constructed with the space group $P1$.

become almost parallel to the c axis as the hole doping is increased to $x=0.185$ ($\phi\sim 15°$) where the coherent JT distortion almost disappears. It is noted that the coherent JT distortion is mainly formed in the ab plane (i.e., the equatorial plane). The spin orientation along the b axis in $La_{0.89}Sr_{0.11}MnO_3$ at 12 K thus indicates a competition between the ferromagnetic ordering and the residual coherent JT distortion. An increased hole concentration leads to a weakened residual coherent JT distortion, and a corresponding spin rotation.

Additional evidence of the correlation between the spin orientation and the coherent JT distortion is observed for the temperature dependence of σ_{JT} and ϕ for $La_{0.835}Sr_{0.165}MnO_3$. Figure 4(a) shows that the $La_{0.835}Sr_{0.165}MnO_3$ sample has a coherent JT distortion transition at $T_{JT}=160$ K in the ferromagnetic region ($T_c=255$ K). It is noted that the coherent JT distortion is very small, $\sigma_{JT}=0.004$ Å, from 255–160 K. One should observe simultaneous transitions for both the spin orientation and coherent JT distortion if they are correlated with one another. Above 160 K where the coherent JT distortion is very small, the refined spin angle ϕ is $\sim$ 18°; thus the spins are almost parallel to the c axis in agreement with the magnitude of spin angle for $La_{0.815}Sr_{0.185}MnO_3$ at 12 K as shown in Fig. 4(b). Clear discontinuities for both ϕ and σ_{JT} occur at the same temperature $T_{JT}=160$ K. ϕ jumps to 40° at 120 K and remains at this value to the lowest temperature, while σ_{JT} reaches its maximum value at $\sim$ 120 K and remains constant to the lowest temperature. Therefore the spin direction and coherent JT distortion are correlated as a function of both temperature and composition.

We should mention that a very weak antiferromagnetic component of $\sim 0.2\mu_B$/Mn, in addition to the ferromagnetic component of $\sim 3.6\mu_B$/Mn, was reported to develop far below T_c in a single crystal study for $La_{0.875}Sr_{0.125}MnO_3$.[20] We did not observe this antiferromagnetic component in $La_{0.89}Sr_{0.11}MnO_3$ or $La_{0.87}Sr_{0.13}MnO_3$ at $\sim$12 K in our powder patterns, probably because it is too small. In addition, a polaron ordered structure was observed at $x\sim 0.125$ for $La_{1-x}Sr_xMnO_3$,[25] indicating a Mn^{3+}-Mn^{4+} spin superstructural configuration. We were also unable to detect any of these superstructure peaks, suggesting that either the peak intensities are weak or the Mn^{3+}-Mn^{4+} superstructural system is not completely ordered.

Finally, we studied the magnetic structure of $La_{0.815}Sr_{0.185}MnO_3$ in the rhombohedral phase. The magnetic structure in the ferromagnetic ordered rhombohedral phase in

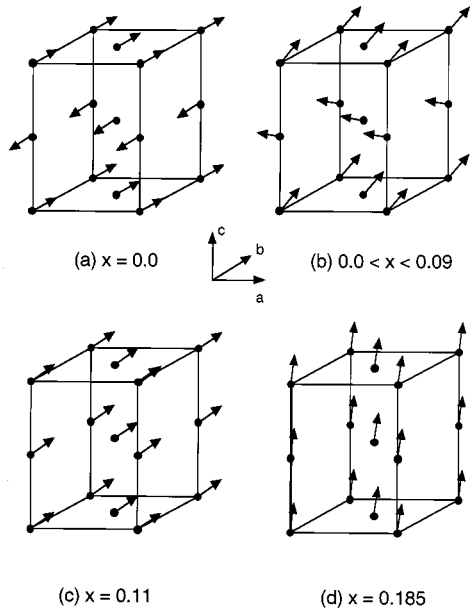

FIG. 10. Illustration of the magnetic structure unit cells in *Pbnm* symmetry as a function of hole concentration x at 12 K for $La_{1-x}Sr_xMnO_3$ ($0.0\leqslant x\leqslant 0.185$): An A-type antiferromagnetic structure with the spin moment along the b axis and the antiferromagnetic coupling along the c axis in the *Pbnm* symmetry for $x=0.0$ (a); a canted A-type antiferromagtic structure with the ferromagnetic component along the c axis for $0.0<x<0.09$ (b); a ferromagnetic structure with spin mainly along the b axis ($x=0.11$) (c), and a ferromagnetic structure with spin almost along the c axis ($x=0.185$) (d).

$LaMnO_{3+\delta}$ ($\delta=0.15$) was reported in Ref. 15, and the spin direction was refined to be in the *ab* plane and alternate between [0 1 0] and [−1 1 0] in successive planes in the $R\bar{3}c$ hexagonal description ($a=\sqrt{2}a_p$, $c=2\sqrt{3}a_p$, $\gamma=120°$). This spin configuration indicates a canted ferromagnetic structure. Our refinements also show that the spin direction is in the *ab* plane in the rhombohedral structure of $La_{0.815}Sr_{0.185}MnO_3$ (from 290–150 K), in agreement with the previously reported result.[15] However, we were unable to uniquely refine the spin direction in the second plane of the unit cell assuming the spins in the first plane are along the [0 1 0] direction. Therefore whether the ferromagnetic structure is canted or not in the rhombohedral structure cannot be determined from this powder-diffraction study.

CONCLUSION

The resulting spin arrangements for $La_{1-x}Sr_xMnO_3$ ($0.0 \leqslant x \leqslant 0.185$) are illustrated in Fig. 10. In the ferromagnetic ordered region ($0.09 < x \leqslant 0.185$), the spin orientation is mainly aligned along the *b* axis in $La_{0.89}Sr_{0.11}MnO_3$ when the residual coherent JT distortion has a finite value of 0.026 Å, while it is mainly along the *c* axis in $La_{0.815}Sr_{0.185}MnO_3$ when the coherent JT distortion almost disappears. This indicates a correlation between the ferromagnetic spin orientation and the coherent JT distortion. The correlation was further demonstrated by the simultaneous transitions for both the spin orientation and the coherent JT distortion upon decreasing temperature in $La_{0.835}Sr_{0.165}MnO_3$. The data confirm the coupling between the structural and magnetic properties in $La_{1-x}Sr_xMnO_3$ ($0.11 \leqslant x \leqslant 0.185$).

ACKNOWLEDGMENTS

The work at NIU was supported by the ARPA/ONR and at ANL by the U.S. Department of Energy, Division of Basic Energy Sciences-Materials Sciences, under Contract No. W-31-109-ENG-38. The authors would like to thank S. Short.

[1] G. H. Jonker and J. H. Van Santen, Physica (Utrecht) **16**, 337 (1950).
[2] S. Jin, Th. H. Tiefel, M. McCormack, R. A. Fastnacht, R. Ramesh, and L. H. Chen, Science **264**, 413 (1994).
[3] A. Urushibara, Y. Moritomo, T. Arima, A. Asamitsu, G. Kido, and Y. Tokura, Phys. Rev. B **51**, 14 103 (1995).
[4] Y. Moritomo, A. Asamitsu, and Y. Tokura, Phys. Rev. B **56**, 12 190 (1997).
[5] A. J. Millis, P. B. Littlewood, and B. I. Shraiman, Phys. Rev. Lett. **74**, 5144 (1995).
[6] H. Y. Hwang, S-W. Cheong, P. G. Radaelli, M. Marezio, and B. Batlogg, Phys. Rev. Lett. **75**, 914 (1995).
[7] Lide M. Rodriguez-Martinez and J. Paul Attfield, Phys. Rev. B **54**, R15 622 (1996).
[8] P. G. Radaelli, G. Iannone, M. Marezio, H. Y. Hwang, S-W. Cheong, J. D. Jorgensen, and D. N. Argyriou, Phys. Rev. B **56**, 8265 (1997).
[9] C. Zener, Phys. Rev. **82**, 403 (1951).
[10] P. W. Anderson and H. Hasegawa, Phys. Rev. **100**, 675 (1955).
[11] P.-G. de Gennes, Phys. Rev. **118**, 141 (1960).
[12] E. O. Wollen and W. C. Koehler, Phys. Rev. **100**, 545 (1955).
[13] Gen Matsumoto, J. Phys. Soc. Jpn. **29**, 606 (1970).
[14] J. B. A. A. Elemans, B. Van Laar, K. R. Van Der Veen, and B. O. Loopstra, J. Solid State Chem. **3**, 238 (1971).
[15] J. A. Alonso, M. J. Martinez-Lope, M. T. Casais, and A. Munoz, Solid State Commun. **102**, 7 (1997).
[16] H. Kawano, R. Kajimoto, M. Kubota, and H. Yoshizawa, Phys. Rev. B **53**, 2202 (1996).
[17] J. Inoue and S. Maekawa, Phys. Rev. Lett. **74**, 3407 (1995).
[18] D. N. Argyriou, J. F. Mitchell, C. D. Potter, D. G. Hinks, J. D. Jorgensen, and S. D. Bader, Phys. Rev. Lett. **76**, 3826 (1996).
[19] H. Kawano, R. Kajimoto, M. Kubota, and H. Yoshizawa, Phys. Rev. B **53**, R14 709 (1996).
[20] L. Pinsard, J. Rodriguez-Carvajal, A. H. Moudden, A. Anane, A. Revcolevschi, and C. Dupas, Physica B **234–236**, 856 (1997).
[21] A. Asamitsu, Y. Moritomo, Y. Tomioka, T. Arima, and Y. Tokura, Nature (London) **373**, 407 (1995).
[22] C. H. Booth, F. Bridges, G. H. Kwei, J. M. Lawrence, A. L. Cornelius, and J. J. Neumeier, Phys. Rev. Lett. **80**, 853 (1998).
[23] B. Dabrowski, X. Xiong, Z. Bukowski, R. Dybzinski, P. W. Klamut, J. E. Siewenie, O. Chmaissen, J. Shaffer, C. W. Kimball, J. D. Jorgensen, and S. Short, Phys. Rev. B **60**, 7006 (1999).
[24] L. Vasilu-Doloc, J. W. Lynn, A. H. Moudden, A. M. de Leon-Guevara, and A. Revcolevschi, J. Appl. Phys. **81**, 5491 (1997).
[25] Y. Yamada, O. Hino, S. Nohdo, and R. Kanao, T. Inami, and S. Katano, Phys. Rev. Lett. **77**, 904 (1996).
[26] B. Dabrowski, K. Rogacki, X. Xiong, P. W. Klamut, R. Dybzinski, J. Shaffer, and J. D. Jorgensen, Phys. Rev. B **58**, 2716 (1998).
[27] J. D. Jorgensen, J. J. Faber, J. M. Carpenter, R. K. Crawford, J. R. Haumann, R. L. Hitterman, R. Kleb, G. E. Ostrowski, F. J. Rotella, and T. G. Worton, J. Appl. Crystallogr. **22**, 321 (1989).
[28] A. C. Larson and R. B. Von Dreele, Los Alamos Internal Report No. 86-748, 1985–1990 (unpublished).
[29] J. Rodriguez-Carvajal, M. Hennion, F. Moussa, and A. H. Moudden, Phys. Rev. B **57**, R3189 (1998).
[30] E. F. Bertaut, Acta Crystallogr., Sect. A: Cryst. Phys., Diffr., Theor. Gen. Crystallogr. **A24**, 217 (1968).